INTERNATIONAL JOURNAL FOR NUMERICAL METHODS IN FLUIDS
Int. J. Numer. Meth. Fluids 2005; **49**:583–602
Published online 11 July 2005 in Wiley InterScience (www.interscience.wiley.com). DOI: 10.1002/fld.994

Direct numerical simulation of turbulent forced convection in a pipe

M. Piller*,†

Dipartimento di Ingegneria Navale del Mare e per l'Ambiente, Università degli studi di Trieste, via A. Valerio 10, 34127, Trieste, Italy

SUMMARY

Direct numerical simulations (DNS) are carried out to study fully developed turbulent pipe flow and heat transfer at Reynolds number $Re_m \approx 5300$ based on bulk velocity and pipe diameter. This paper provides detailed information on the mean properties and turbulence statistics up to fourth order, the budget and the wavenumber spectra of the temperature fluctuations, for three different wall boundary conditions. To investigate the differences between fully developed turbulent heat transfer in axisymmetric pipe and plane channel geometry, the present DNS results are compared to those obtained from channel flow simulations. The differences between channel and pipe flow statistics are modest and reveal that the temperature fluctuations in the pipe are slightly more intense. The present results show that the mean temperature profile does not conform to the accepted law of the wall. The boundary conditions affect the turbulence statistics both in the near-wall and core regions; this observation complements previous studies concerning different flow and heat transfer configurations. Copyright © 2005 John Wiley & Sons, Ltd.

KEY WORDS: DNS; heat transfer; turbulence; pipe; thermal boundary conditions

1. INTRODUCTION

Direct numerical simulations (DNS) are carried out to study fully developed turbulent pipe flow and heat transfer at Reynolds number $Re_m \approx 5300$ based on bulk velocity and pipe diameter. Ideal isothermal, ideal isoflux and *mixed* boundary conditions are considered; they are referred to as IWT, IWHF and MT, respectively. The flow is driven by a constant pressure gradient and the friction Reynolds number, based on the pipe diameter, is $Re^* = 360$; the Prandtl number of the fluid is 0.71. Buoyancy effects are neglected. The present study provides

*Correspondence to: M. Piller, Dipartimento di Ingegneria Navale del Mare e per l'Ambiente, Università degli studi di Trieste, via A. Valerio 10, 34127, Trieste, Italy.
†E-mail: piller@univ.trieste.it

Contract/grant sponsor: MIUR-PRIN 2001

Received 23 December 2004
Revised 15 March 2005
Accepted 20 March 2005

detailed information on the mean properties and turbulence statistics up to fourth order, the budget and the wavenumber spectra of the temperature fluctuations.

Several DNS studies have been focusing on the passive thermal field in a plane channel flow, covering a relatively wide range of Reynolds and Prandtl numbers and a variety of temperature wall boundary conditions. Kim *et al.* [1] simulated a turbulent channel flow at $Re_h^* = 180$ and $Pr = 0.71$, assuming that a passive scalar is uniformly generated within the fluid and removed from the isothermal walls. A DNS of fully developed thermal field in a channel flow with the MT condition, at $Re_h^* = 150$, $Pr = 0.7$, was carried out by Kasagi *et al.* [2]. Tiselj *et al.* [3] presented a DNS investigation of the turbulent heat transfer in a flume, with both an isoflux condition, similar to the IWHF used in this study, and the MT condition. Their results show that the mean temperature profile is not sensibly affected by the type of boundary condition, while significant differences exist in the near-wall instantaneous temperature fields. In addition, they show that the influence of the different boundary conditions weakens as the Prandtl number increases, since most of the change in temperature occurs in the progressively thinner thermal boundary layer. The results by Kong *et al.* [4] for a turbulent thermal boundary layer, with both isoflux and isothermal boundary conditions, agree with the observations by Tiselj *et al.* [3], in that the influence of the temperature boundary conditions is confined to the range $y^+ < 10$. Piller *et al.* [5] carried out several DNS for the channel flow with the two walls kept at constant, different temperatures, for $Re_h^* = 150$ at $Pr = 0.025, 0.05, 0.1, 0.3$ and 1.0. More recently, Seki *et al.* [6] compared the turbulence temperature statistics for channel flows at two Reynolds numbers, with two different boundary conditions: constant temperature difference between top and bottom surfaces and MT conditions. They evidence relevant differences between the results for the two cases in the near-wall and core regions.

A major contribution of the present study consists in a better characterization of three types of wall thermal conditions. The similarity of the resulting temperature fields is synthetically quantified by the mutual correlation coefficient. The influence of the wall thermal conditions is shown to extend to the entire temperature field; the damping of the temperature fluctuations at the wall, characteristic of isothermal conditions, affects the temperature statistics in the inner layer, while most of the dissimilarities, observed in the core region, can be ascribed to the different axial distribution of the wall heat flux. The studies by Tiselj *et al.* [3] and by Kong *et al.* [4] do not take into account *ideal* isothermal conditions, IWT; accordingly, their results reveal only near-wall effects of the different boundary conditions.

To investigate the differences between fully developed turbulent heat transfer in axisymmetric pipe and plane channel geometry, the present DNS results are compared to those obtained from channel flow simulations. The differences between channel and pipe flow results are modest and reveal that the temperature fluctuations in the pipe are slightly more intense.

2. GOVERNING EQUATIONS

Incompressible flow in pipes can be described by the Navier–Stokes equations in cylindrical coordinates. By assuming constant fluid properties, negligible viscous energy dissipation and absence of internal heat generation and using the following dimensionless quantities:

$$\hat{r} = \frac{r}{D}, \quad \mathbf{u}^+ = \frac{\mathbf{u}}{u^*}, \quad p^+ = \frac{p'}{\rho u^{*2}}, \quad \hat{t} = \frac{tu^*}{D}, \quad Re^* = \frac{u^* D}{\nu}$$

the dimensionless continuity and momentum equations result in:

$$\hat{\nabla}\cdot\mathbf{u}^+ = 0 \tag{1}$$

$$\frac{D\mathbf{u}^+}{D\hat{t}} = -\hat{\nabla}p^+ + \frac{1}{Re^*}\hat{\nabla}^2\mathbf{u}^+ + 4\mathbf{e}_1 \tag{2}$$

$$\mathbf{u}^+|_{\hat{r}=1/2} = \mathbf{0} \tag{3}$$

$$\mathbf{u}^+(\hat{x}+\hat{L},\hat{r},\varphi) = \mathbf{u}^+(\hat{x},\hat{r},\varphi) \tag{4}$$

where no-slip boundary conditions have been enforced on the pipe wall. The velocity field is periodic along the streamwise direction $\mathbf{e}_1$ and the flow is driven by a constant pressure gradient. The instantaneous pressure gradient is split into a mean value $-\nabla p$, which balances the viscous friction at the wall and equals 4 when scaled with D and u^*.

2.1. Wall thermal conditions

Three boundary conditions for the temperature field are formalized and discussed in some detail. Specific issues, concerning their implementation in a finite volume algorithm, are also addressed.

2.1.1. Ideal isoflux boundary conditions. The ideal isoflux conditions, IWHF hereafter, assume that the instantaneous wall heat flux is both uniform in space and constant in time. This implies that the time-averaged temperature varies linearly with x [7]. By introducing the following dimensionless temperature:

$$\vartheta^+ = \frac{\bar{T}_w(x) - T(x,r,\varphi,t)}{T^*}, \quad \frac{\partial\bar{\vartheta}^+}{\partial\hat{x}} = 0 \tag{5}$$

where T^* is the friction temperature, the instantaneous energy equation can be cast as

$$\frac{\partial\vartheta^+}{\partial\hat{t}} + \hat{\nabla}\cdot(\mathbf{u}^+\vartheta^+) = \frac{1}{Pe^*}\hat{\nabla}^2\vartheta^+ + 4\frac{u_x^+}{u_m^+} \tag{6}$$

where u_m^+ is the bulk velocity

$$u_m^+ = \frac{1}{A_c}\int_{A_c}\bar{u}_x^+\,\mathrm{d}A$$

with A_c the normal cross-flow area of the pipe. The friction Péclet number is defined as $Pe^* = u^*D/\alpha$, being α the thermal diffusivity of the fluid. Periodic boundary conditions can be applied to the instantaneous quantity $\vartheta^+(\hat{x},\hat{r},\varphi,\hat{t})$. The dimensionless IWHF wall thermal condition is defined by

$$\left.\frac{\partial\vartheta^+}{\partial\hat{r}}\right|_w = -Pe^* \tag{7}$$

Sommer *et al.* [8] point out that the energy equation with IWHF conditions is ill-posed. The non-uniqueness of the solution can be removed by the following integral energy-conservation

constraint:

$$\frac{\partial \Theta^+}{\partial t} = 0, \quad \Theta^+ = \frac{1}{V}\int_V \vartheta^+ \, \mathrm{d}V \tag{8}$$

where V denotes the computational domain. A consistent finite-volume method enforces automatically constraint (8), since it is based on local integral balance equations.

2.1.2. Ideal isothermal conditions. General isothermal conditions assume that the time-averaged wall temperature is uniform, resulting in an exponential variation of the time-averaged temperature difference [7],

$$\bar{T}_w - \bar{T} = (\bar{T}_w - \bar{T})_{x=0} \mathrm{e}^{-ax}, \quad \frac{\partial \bar{\vartheta}^+}{\partial x} = 0 \tag{9}$$

where a is an unknown parameter. The ideal isothermal conditions, IWT hereafter, assume that the wall temperature is both uniform and constant, which implies $\vartheta^+ = 0$ at the wall. The conservation equation for the dimensionless temperature ϑ^+, complemented with appropriate boundary conditions, reads

$$\frac{\partial \vartheta^+}{\partial \hat{t}} + \hat{\nabla} \cdot (\mathbf{u}^+ \vartheta^+) = \frac{1}{Pe^*} \hat{\nabla}^2 \vartheta^+ + \hat{a} \vartheta^+ u_x^+ - \frac{1}{Pe^*} \left[2\hat{a} \frac{\partial \vartheta^+}{\partial \hat{x}} - \hat{a}^2 \vartheta^+ \right] \tag{10}$$

$$\vartheta^+ = 0 \quad \text{at } \hat{r} = 1/2 \tag{11}$$

$$\vartheta^+(\hat{x} + \hat{L}, \hat{r}, \varphi, \hat{t}) = \vartheta^+(\hat{x}, \hat{r}, \varphi, \hat{t}) \tag{12}$$

At each instant in time, Equations (10)–(12) can be interpreted as a quadratic eigenvalue problem. The unique eigenvalue, corresponding to the physical solution, can be determined by solving the following quadratic algebraic equation, resulting from the integration of (10) on the computational domain:

$$(\bar{\Theta}^+ St_D^*)\hat{a}^2 + (Pe^* \bar{u}_m^+)\hat{a} - 4Nu_D = 0, \quad St_D^* = \frac{Nu_D}{Pe^*} \tag{13}$$

where the Nusselt number Nu_D is defined in the usual way, with respect to the local temperature difference $T_w - \bar{T}_m(x)$. It can be shown [7] that Nu_D is constant along x, thus eliminating any ambiguity in its use as a global parameter. Since the time-averaged wall heat flux is not known, moving averages can be used in order to approximate the terms $\bar{\Theta}^+$, St_D^* and Nu_D. With reference to steady flows, a similar method was originally proposed by Patankar *et al.* [9].

An alternative solution method can be devised by defining a different dimensionless temperature:

$$\Psi(\hat{x}, \hat{r}, \varphi, \hat{t}) = \frac{\bar{T}_w - T(\hat{x}, \hat{r}, \varphi, \hat{t})}{\bar{T}_m(\hat{x} = \hat{L}) - \bar{T}_m(\hat{x} = 0)}, \quad \frac{\partial \bar{\Psi}}{\partial \hat{x}} \propto \mathrm{e}^{-\hat{a}\hat{x}} \neq 0 \tag{14}$$

which is related to ϑ^+ as

$$\vartheta^+(\hat{x}, \hat{r}, \varphi, \hat{t}) = \frac{1}{St_D^*} \frac{\Psi(\hat{x}, \hat{r}, \varphi, \hat{t})}{\bar{\Psi}_m(\hat{x})} \tag{15}$$

The following proportionality condition can be derived for the dimensionless temperature:

$$\Psi(\hat{x}=\hat{L},\hat{r},\varphi,\hat{t})=\gamma\Psi(\hat{x}=0,\hat{r},\varphi,\hat{t}) \tag{16}$$

where

$$\gamma=\frac{\bar{\Psi}_m(\hat{x}=\hat{L})}{\bar{\Psi}_m(\hat{x}=0)}=\frac{\bar{\Psi}_m(0)-1}{\bar{\Psi}_m(0)}=\mathrm{e}^{-\hat{a}\hat{L}} \tag{17}$$

The unknown parameter γ is computed directly from its definition (17), using a running average for approximating the time-averaged, dimensionless inlet bulk temperature $\bar{\Psi}_m(0)$. The dimensionless energy equation reads, in this case:

$$\frac{\partial\Psi}{\partial\hat{t}}+\hat{\nabla}\cdot(\mathbf{u}^{+}\Psi)=\frac{1}{Pe^{*}}\hat{\nabla}^{2}\Psi \tag{18}$$

$$\Psi=0 \quad \text{at } \hat{r}=1/2 \tag{19}$$

$$\Psi(\hat{x}+\hat{L},\hat{r},\varphi,\hat{t})=\gamma\Psi(\hat{x},\hat{r},\varphi,\hat{t}) \tag{20}$$

The main advantage of formulation (10)–(12) consists in that the periodic boundary conditions can be enforced in their standard form, allowing for an efficient solution process along the streamwise direction. The results, reported in this paper, have been obtained by the second approach.

2.1.3. Mixed-type boundary conditions. With the mixed-type boundary conditions, MT hereafter, the time-averaged wall heat flux is uniform in space, while the instantaneous wall temperature is constant with time. An energy balance shows that the wall temperature varies linearly along the streamwise direction. By using the dimensionless temperature ϑ^{+} the resulting energy equation is identical to (6), but the boundary condition (7) is replaced by (11).

2.2. Numerical methodology

The continuity, momentum and energy equations in cylindrical coordinates are solved using a symmetric second-order finite-volume method. The axis singularity is circumvented by computing the cartesian velocity components on the pipe axis by a least-square approximation, based on the nearest cylindrical velocity components [10]. The time-integration is based on a fully implicit, three-step predictor–corrector algorithm [11]. The alternate direction implicit (ADI) method [12] is used to decouple the coordinate directions, for the solution of the momentum and energy equations. The momentum and continuity equations are decoupled by the Projection 2 method proposed by Gresho [13]. The computational grid consists of $111\times180\times324$ control volumes along the radial, azimuthal and axial directions, respectively; the streamwise domain length is $L_x/D=6.328$. The appropriate grid resolution was selected by conforming to the criteria proposed by Grötzbach [14] and was tested by comparison with previous simulations for the flow field [15, 16].

3. TURBULENCE STATISTICS

3.1. Mean flow properties

Some mean flow properties are reported in Table I. The Reynolds number and the friction factor are in good agreement with DNS results reported by Eggels *et al.* [16] and by Fukagata *et al.* [15] and with Colebrook's empirical formula [17]. The calculated Nusselt number depends weakly on the wall thermal conditions, with a relative 6% difference of the average Nusselt number, between the maximum MT value and the minimum IWT result. The Nusselt number obtained from the Gnielinski's correlation [17] is in excellent agreement with the IWT result. Twice the ratio between the Stanton number and the friction factor is close to unity for the three temperature fields, denoting substantial Reynolds' similarity between the velocity and temperature fields, in particular for the IWT case.

The considered boundary conditions affect the mean temperature distribution, reported in Figure 1; the IWHF and MT profiles are very close to each other, as already found by Tiselj *et al.* [3] for a turbulent flume flow and Kong *et al.* [4] for a turbulent boundary layer. The IWT profile is sensibly higher than the others in the core region. Compared to the channel flow with MT conditions, the axisymmetric flow configuration leads to a larger wall-normal turbulent heat flux and, consequently, to a larger temperature difference, with all the three considered boundary conditions. The circumstance that the IWHF and MT mean temperature profiles are almost coincident, while sensibly different from the IWT case, can be ascribed to the different source terms, appearing in the corresponding energy equations. These source terms express the mean and turbulent axial advection and the mean axial diffusion of heat, caused by the mean-temperature variation along the streamwise direction. The elimination of the wall temperature fluctuations, on the other hand, does not seem to affect the mean temperature profile sensibly, as can be inferred by the substantial coincidence of the MT and IWHF profiles. A mean energy balance can be derived by time-averaging equations (6) and (10):

$$\frac{1}{Pe^*}\,\frac{1}{\hat{r}}\,\frac{\mathrm{d}}{\mathrm{d}\hat{r}}\left(\hat{r}\,\frac{\mathrm{d}\bar{\vartheta}^+}{\mathrm{d}\hat{r}}\right)=\frac{1}{\hat{r}}\,\frac{\mathrm{d}}{\mathrm{d}\hat{r}}(\hat{r}\overline{u_r^{+\prime}\vartheta^{+\prime}})+S_\vartheta^+ \tag{21}$$

where

$$S_\vartheta^+=\begin{cases}-4\,\dfrac{\bar{u}_x^+}{u_m^+} & \text{IWHF and MT}\\[2ex] -\hat{a}\left[\bar{u}_x^+\bar{\vartheta}^+ + \overline{u_x^{+\prime}\vartheta^{+\prime}} + \dfrac{\hat{a}}{Pe^*}\,\bar{\vartheta}^+\right] & \text{IWT}\end{cases} \tag{22}$$

The various terms in Equation (22) can be interpreted as follows:

(a) $4\bar{u}_x^+/u_m^+$: mean advection term, for the IWHF and MT conditions.
(b) $\hat{a}\overline{u_x^{+\prime}\vartheta^{+\prime}}$: turbulent axial advective heat flux. The (dimensional) turbulent temperature fluctuations tend to weaken moving along the streamwise direction, since the temperature difference between the wall and the fluid becomes smaller. This causes a net positive turbulent advective flux in the streamwise direction.

Table I. Mean flow properties.

Case	Re_m	$C_f \times 10^3$	Nu_D	$St_D \times 10^3$	K_ϑ	B_ϑ
IWHF	5273	9.32	18.32	4.89	0.33	2.0
IWT	5273	9.32	17.44	4.66	0.28	0.4
MT	5273	9.32	18.54	4.95	0.34	2.0
Reference [16]	5300	9.22				
Reference [15]	5310	9.19				
Correlations		9.21	17.51	4.68	0.48	3.9

The last row reports the friction factor and the Nusselt number obtained from empirical correlations. The friction factor was derived by the Colebrook's equation; the Nusselt number was obtained from the Gnielinski's correlation.

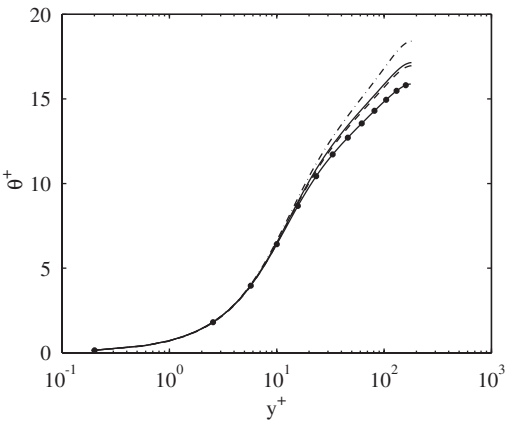

Figure 1. Mean temperature profiles: ——: IWHF; – – –: MT; —— · ——: IWT; —●—: channel at $Re_h^* = 180$, $Pr = 0.71$ with MT wall temperature conditions.

(c) $\hat{a}\bar{u}_x^+\bar{\vartheta}^+$: mean advective heat flux for the IWT case, corresponding to the term (a) for the other cases.
(d) $(\hat{a}^2/Pe^*)\bar{\vartheta}^+$: mean streamwise thermal diffusion, due to the axial curvature of the mean temperature profile.

By integrating Equation (21)

$$\bar{\vartheta}^+(\hat{r}) = -Pe^* \int_{\hat{r}}^{1/2} \overline{u_r^{+\prime}\vartheta^{+\prime}}\, \mathrm{d}\hat{r}' - Pe^* \int_{\hat{r}}^{1/2} \frac{1}{\hat{r}'} \int_0^{\hat{r}'} \hat{r}'' S_\vartheta^+(\hat{r}'')\, \mathrm{d}\hat{r}''\, \mathrm{d}\hat{r}' \tag{23}$$

By inspection of the various contributions in (23), not reported here, it was recognized that the turbulent axial advective flux (b) and the mean streamwise thermal diffusion (d) are orders of magnitude smaller than the other contributions, for the IWT case. The larger values of the mean temperature for the IWT case, compared to the other types of boundary conditions, are due to a larger positive difference between the mean axial advective and the radial turbulent heat fluxes.

Best fit logarithmic profiles are obtained, corresponding to the coefficients reported in the last two columns of Table I. The thermal boundary condition has a strong effect on the value of the Kader's constant k_ϑ, which is sensibly lower than the values of 0.48 obtained by Subramanian *et al.* [18] for a turbulent boundary layer and 0.45 from measurements in an electrically heated pipe obtained by Johnk *et al.* [19]. Na *et al.* [20], in their simulations of a turbulent channel flow at $Re_h^* = 150$, with the two walls kept at constant, different temperatures, report calculated values of k_ϑ as 0.22, 0.21 and 0.23 at $Pr = 1.0$, 3.0 and 10.0, respectively. Kawamura *et al.* [21], based on DNS data for turbulent channel flow with MT wall thermal conditions at $Re_h^* = 180$ and 395, show that the value of k_ϑ increases with increasing Reynolds number, and propose a best-fit value of 0.43 for the highest considered Reynolds number.

3.2. Turbulence intensity

The rms temperature fluctuations are shown in Figure 2; the statistics for a plane channel flow at $Re_h^* = 180$, with MT conditions, are reported for comparison [22]. The IWHF temperature fluctuations present a plateau in the conduction sublayer, where the fluctuation intensity accounts to approximately 83% of the peak value. The IWT and MT temperature fluctuations vanish at the wall. As a consequence, in the near-wall region, $y^+ < 15$, the IWHF temperature fluctuations are sensibly more intense than the IWT and MT ones. For $y^+ > 15$ the temperature fluctuations for the IWT case are the most intense, while the intensity of the IWHF and MT temperature fluctuations is comparable for $y^+ > 30$, in agreement with findings by both Kong *et al.* [4] and Tiselj *et al.* [3], who do not report any significant effect of the thermal wall boundary conditions on the temperature fluctuations for $y^+ > 10$. This behaviour is consistent with the larger production term for the IWT temperature fluctuations, compared to the other cases, as evident in Figure 8(a). The decrease of the turbulent temperature fluctuations towards the centreline is due to the symmetry of the imposed thermal boundary conditions, which cause the vanishing of the production term, approaching the centreline. The results for the channel flow by Abe *et al.* [22, 23], with imposed MT conditions, agree with the MT results for the pipe flow for $y^+ < 20$, while at larger distance from the wall the temperature fluctuations for the pipe flow are slightly more intense.

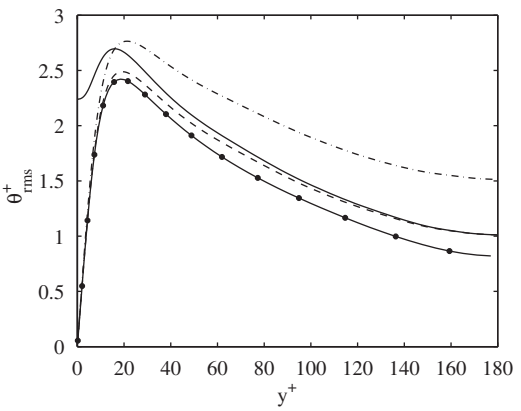

Figure 2. The rms temperature profiles: ——: IWHF; – – –: MT; —— · ——: IWT; —●—: channel at $Re_h^* = 180$, $Pr = 0.71$ with MT wall temperature conditions.

3.3. *Visualization of instantaneous near-wall coherent structures*

The effect of the different thermal boundary conditions on the instantaneous temperature field is investigated by comparing contours of instantaneous temperature and streamwise velocity on cross-flow planes, reported in Figures 3. By comparing Figures 3(a), 3(c) and 3(d) it can be observed that there is a remarkable similarity between the MT and IWT temperature fields with the streamwise velocity component, in the viscous wall region. The no-slip condition for the velocity field and the isothermal condition for the temperature field cause large velocity and temperature gradients at the edge of the viscous and conductive sublayers, respectively, as evident also in Figure 2. This feature has already been observed, among others, by Chen *et al.* [24] in their study of turbulent structures in a turbulent boundary layer and by Tiselj *et al.* [3] in a DNS of turbulent flow in a flume. In the present study, the comparison is extended to the IWT temperature field. From Figure 3(b) it can be seen that the near-wall similarity between u_x^+ and ϑ^+ is lost when the IWHF condition is enforced and a well definite temperature front [3] cannot be recognized. The difference between the near-wall profiles of

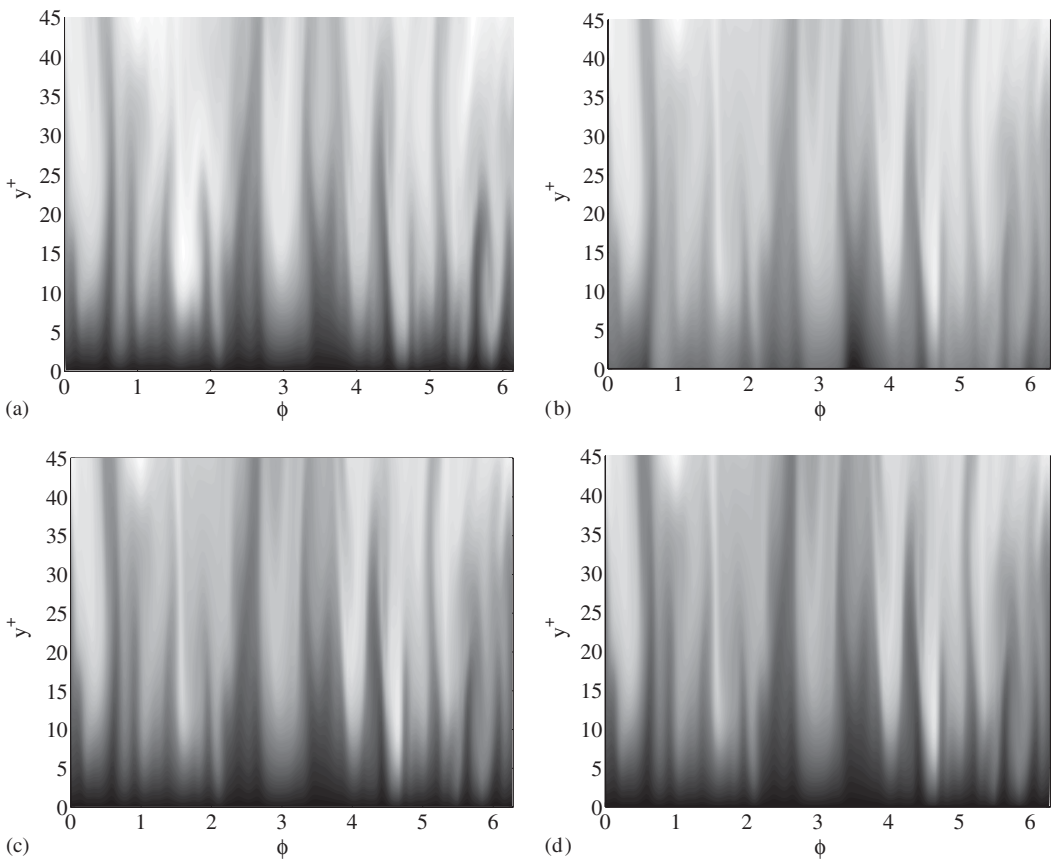

Figure 3. Instantaneous contours of: (a) streamwise velocity and (b)–(d) temperature, on a $r - \varphi$ plane; (b) IWHF; (c) MT; and (d) IWT.

u_x^+ and ϑ^+, for the IWHF case, reflects in the lower u_x–ϑ correlation coefficient inside the inner layer, reported in Figure 5.

3.4. Turbulent heat fluxes

The radial turbulent heat flux is reported in Figure 4(a). For $y^+ < 10$ all the profiles are close to each other, but in the conduction sublayer the IWHF profile decays slower, since more intense turbulent thermal fluctuations can reach the wall. In the outer layer the turbulent heat flux for the IWT case is sensibly higher than for the other boundary conditions. The IWHF and MT heat fluxes are quite similar and slightly more intense than for the channel flow by Abe *et al.* [22, 23], with MT conditions. This feature suggests that, out of the inner layer, the damping of the temperature fluctuations at the wall is less relevant than the streamwise distribution of the wall heat flux, resulting in different source terms in the energy equation. Tiselj *et al.* [3] report that, in a turbulent flume flow, there is almost no difference in the wall-normal turbulent heat flux when using either MT or IWHF conditions, both at $Pr = 1$ and 5.4, for $y^+ > 10$, while for $y^+ < 10$ they find larger values of the turbulent heat flux for the IWHF condition.

The axial turbulent heat flux is reported in Figure 4(b). In the conductive sublayer the relative magnitude of the profiles is IWHF > IWT > MT, while farther from the wall IWT > IWHF > MT, as for the radial turbulent heat flux. Out of the inner layer the IWHF and MT profiles are very close to each other and sensibly lower than the IWT result, confirming that, in this region, the damping of the near-wall temperature fluctuations is less effective than the different wall heat flux distribution. The axial turbulent heat flux is not affected by the flow configuration, as can be inferred by the coincidence of the MT results for the pipe and channel flows.

The correlation coefficients $R_{u_r\vartheta}$ and $R_{u_x\vartheta}$ are shown in Figure 5. Tiselj *et al.* [3] report that the MT and IWHF thermal boundary conditions lead to very similar results for these coefficients, except for $y^+ < 10$. The same features can be recognized for the pipe flow. In the inner layer, the IWT and MT coefficients are almost coincident, while the IWHF coefficients decay faster towards the wall, due to the difference in the wall boundary conditions imposed on the temperature and velocity fields. The flow configuration has a weak effect, resulting in slightly larger correlation coefficients for the channel flow. The correlation coefficients can be used to interpret the relative intensity of the turbulent heat fluxes, with different boundary conditions. Out of the inner layer there are no significant differences in the radial correlation coefficients, so that the different distributions of the radial turbulent heat flux are mainly due to the different intensity of the temperature fluctuations. In the inner layer, the MT and IWT temperature fluctuations are strongly damped due to the presence of the isothermal wall, while the intensity of the IWHF temperature fluctuations is not reduced; on the contrary, the reduction of the $R_{u_r\vartheta}$ correlation coefficient is stronger for the IWHF case; these opposite trends result in quite similar radial turbulent heat fluxes for the three considered temperature fields, in the inner layer. The corresponding axial quantities behave similarly to the radial ones; however, the reduction of the IWHF axial correlation coefficient in the inner layer is relatively modest; as a consequence, the large intensity of the IWHF temperature fluctuations in the inner layer leads to a larger axial turbulent heat flux in this region, compared to the other cases. Figure 6 shows the turbulent Prandtl number; Pr_t for the IWHF profile tends to zero towards the wall, while it tends to a finite value around unity for the other boundary

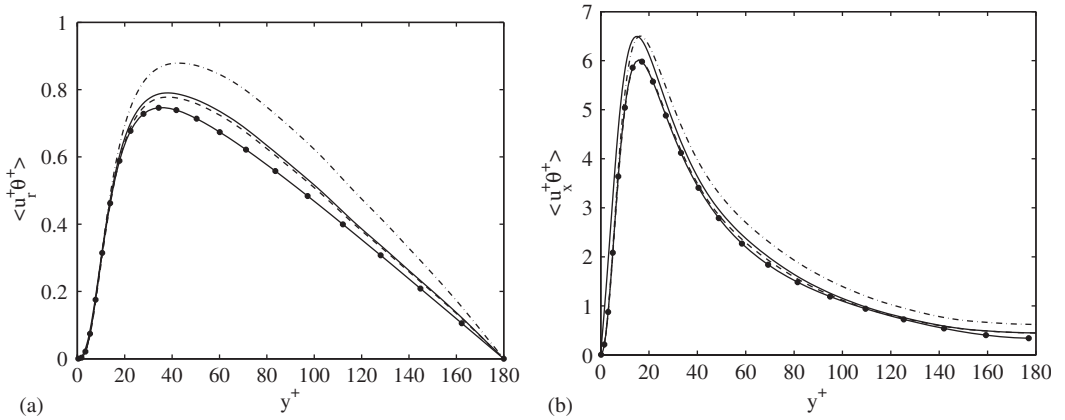

Figure 4. (a) Radial; and (b) axial turbulent heat flux. ——: IWHF; – – –: MT; —— · ——: IWT; —●—: channel at $Re_h^* = 180$, $Pr = 0.71$ by Abe *et al.* [22, 23].

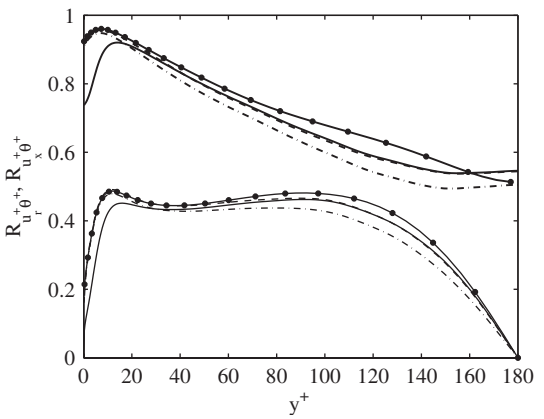

Figure 5. Correlation coefficient between the temperature fluctuations and the fluctuations of the radial (thin lines) and the axial (thick lines) velocity components. ——: IWHF; – – –: MT; —— · ——: IWT; —●—: channel at $Re_h^* = 180$, $Pr = 0.71$ by Abe *et al.* [22, 23].

conditions. The turbulent Prandtl number remains close to unity for $y^+ < 50$, while it decreases to $Pr_t \approx 0.65$ at the centreline. Na *et al.* [20] show that $Pr_t \approx 1$ for $y^+ < 28$, in a channel flow with two walls kept at constant, different temperature, with $Re_h^* = 150$ and $Pr = 1, 3, 10$. In addition, they obtain $Pr_t \approx 0.87$ in the central region of the channel for $Pr = 1$, which is larger than the present results.

3.5. Skewness and kurtosis

Figure 7(a) reports the skewness of the velocity components and of the three temperature fields, considered in the present study. For comparison, the experimental data for a turbulent pipe flow of air are reported [25]. The skewness factors of the three temperature fields are

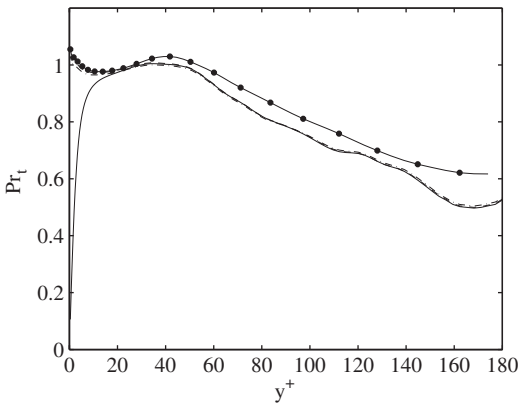

Figure 6. Turbulent Prandtl number. Turbulent diffusivity. ——: IWHF; – – –: MT; —— · ——: IWT; —●—: channel at $Re_h^* = 180$, $Pr = 0.71$ by Abe *et al.* [22, 23].

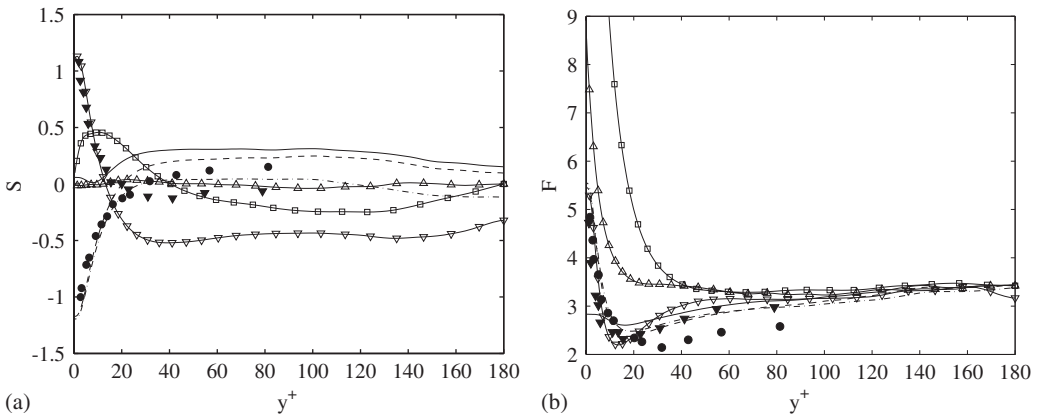

Figure 7. (a) Skewness; and (b) kurtosis of velocity components and temperature. ——: S_ϑ, F_ϑ for IWHF; – – –: S_ϑ, F_ϑ for MT; — · —: S_ϑ, F_ϑ for IWT; —□— : S_{u_r}, F_{u_r}; —△—: S_{u_φ}, F_{u_φ}; —▽—: S_{u_x}, F_{u_x}; ● ● ●: S_ϑ, F_ϑ by Elena [25]; ▼▼▼: S_{u_x}, F_{u_x} by Elena [25].

strongly affected by the boundary conditions, both in the near wall and in the core regions. The results by Tiselj *et al.* [3] for the MT and IWHF conditions are close to each other for $y^+ > 40$. The present MT profile shows some similarity with the corresponding results by Tiselj *et al.* [3], in that S_ϑ is negative in the inner layer, while beyond $y^+ \approx 20$ it tends to become constant and positive. The skewness of the IWHF temperature field is positive and almost constant for $y^+ > 20$, as for the IWHF results by Tiselj *et al.* However, the near-wall behaviour is different, since the present DNS data do not present a positive plateau for $y^+ < 10$, but reach a minimum negative value at $y^+ \approx 9.0$ and then increase approaching the wall. The skewness of the IWT temperature field agrees with the MT results for $y^+ < 10$; beyond this distance, the quantitative agreement is lost and the IWT profile attains smaller

positive values. The experimental data by Elena [25] are in excellent quantitative agreement with the present IWT results. The large negative values of S_ϑ for the MT and IWT temperature fields, for $y^+ < 20$, are consistent with the large positive values of S_{u_x} and S_{u_r}, which denote the presence of intense sweep events. The lower correlation between u_r and u_x with ϑ, for the IWHF case, accounts for the different near-wall behaviour of S_ϑ, in this case. In the outer region, $y^+ > 40$, the most intense radial velocity fluctuations are predominantly directed towards the centreline; consistently, the three temperature skewness factors become positive.

Figure 7(b) shows the kurtosis of the velocity components and of the three temperature fields. The experimental data by Elena [25] for F_ϑ are in relatively good agreement with the IWT result in the near-wall region. The kurtosis of all velocity components and of the MT and IWT temperature fields increases sharply approaching the wall, due to the wall-blocking effect; due to the low correlation between the radial velocity and the IWHF temperature fluctuations, the IWHF flatness does not present relevant variations approaching the wall and attains an approximately constant value of 3 in the viscous wall region, corresponding to the normal distribution. The flatness of all temperature fields exceeds the value of 3 at the centreline. As already found by Elena [25], the flatness of both u_x and ϑ, for the MT and IWT cases, presents a minimum value around 2.0, near the location where the corresponding skewness factor crosses the zero. Elena relates this feature to the presence of harmonic fluctuations, corresponding to $S = 0$ and $F = 1.5$, related to the hydrodynamic instability evidenced by Blackwelder *et al.* [26] in this region. The IWHF temperature also attains a minimum in the flatness factor, in the region of minimum skewness.

3.6. Budget of temperature fluctuations

The conservation equation for the dimensionless temperature variance k_ϑ^+ reads:

$$\frac{\bar{\mathrm{D}} k_\vartheta^+}{\bar{\mathrm{D}} t} = P_{k_\vartheta} + T_{k_\vartheta} + D_{k_\vartheta} + \varepsilon_{k_\vartheta} + S_{k_\vartheta} \tag{24}$$

where P_{k_ϑ}, T_{k_ϑ}, D_{k_ϑ} and $\varepsilon_{k_\vartheta}$ denote the production, turbulent transport, diffusive transport and dissipation terms, respectively. The source term S_{k_ϑ} results from the non-dimensionalization of the energy equation and contains contributions from the other terms. In this context it was decided to gather these contributions in a single term, since it represents the direct effect of the mean temperature axial variation.

$$S_{k_\vartheta} = \begin{cases} \hat{a}\left[2\bar{u}_x^+ k_\vartheta^+ + \bar{\vartheta}\,\overline{u_x^{+\prime}\vartheta^{+\prime}} + \overline{u_x^{+\prime}\vartheta^{+\prime}\vartheta^{+\prime}} - \dfrac{2}{Pe^*}\dfrac{\partial k_\vartheta^+}{\partial \hat{x}} + \dfrac{2}{Pe^*}\hat{a} k_\vartheta^+\right] & \text{IWT} \\ 4\,\dfrac{\overline{u_x^{+\prime}\vartheta^{+\prime}}}{u_m^+} & \text{IWHF, MT} \end{cases} \tag{25}$$

The terms in the budget of k_ϑ^+ are reported in Figures 8(a)–8(d). The present results are compared with statistics for the channel flow at $Re_h^* = 180$, $Pr = 0.71$ by Abe *et al.* [22, 23], with imposed MT conditions. The wall thermal conditions have a non-negligible effect on all terms. The direct effect of the mean temperature axial variation is small compared to the other terms and is not shown. While S_{k_ϑ} for the MT and IWHF conditions is almost coincident and acts as a source term, decreasing monotonically from a near-wall peak value towards the

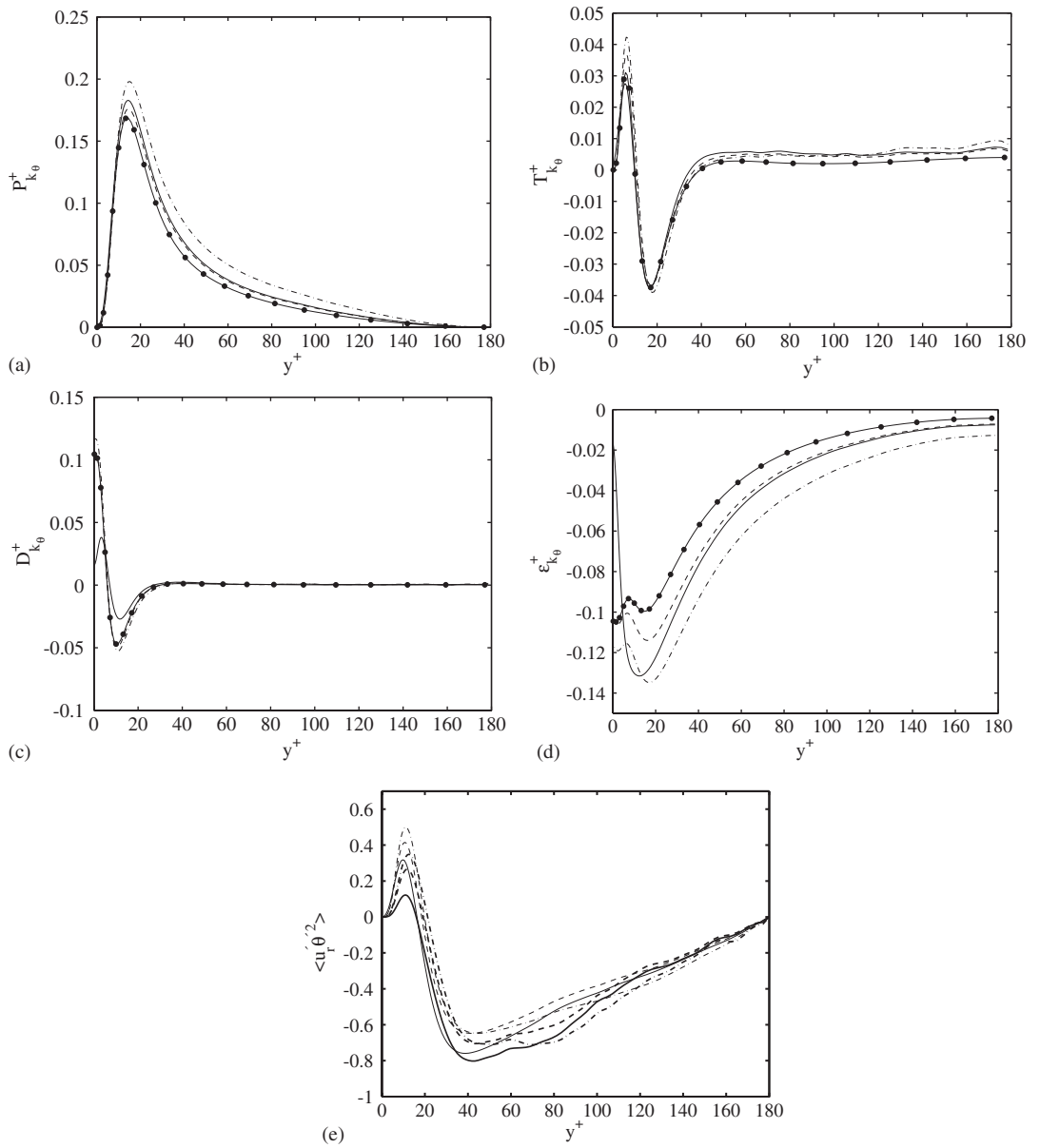

Figure 8. Budget of k_ϑ^+: (a) production; (b) turbulent transport; (c) molecular diffusion; (d) dissipation; (e) gradient-diffusion model for the turbulent transport. ——: IWHF; – – –: MT; —— · ——: IWT; —●–: channel at $Re_h^* = 180$, $Pr = 0.71$ by Abe *et al.* [22, 23]. In (e) thin lines correspond to DNS data, thick lines to the gradient-diffusion model.

centreline, the IWT result is characterized by a non-monotonic behaviour, due to the negative contribution of the axial turbulent transport term $\overline{u_x^{+\prime}\vartheta^{+\prime}\vartheta^{+\prime}}$. Production and dissipation are the dominant contributions across the pipe. The turbulent transport and molecular diffusion terms have a relevant effect for $y^+ < 30$ and, limited to the turbulent transport, in the core region, where it balances the dissipation term. The production term for the IWT case is more intense than for the other cases; noteworthy, the MT production is the smallest, giving additional evidence to the observation that the MT conditions cannot be used to represent *ideal* isothermal conditions. The production for the channel flow with MT conditions is slightly smaller than the corresponding pipe flow result.

The turbulent transport term has a positive peak at $y^+ \approx 5.5, 6.1, 6.1$ and a negative peak at $y^+ \approx 16.9, 17.7, 18.6$, for the IWHF, MT and IWT cases, respectively. It drains temperature fluctuations from the region where production is most intense and conveys them both towards the wall and the core region. For $y^+ > 50$ the turbulent transport term shows a positive plateau and balances production and dissipation. The MT and IWT results are very close to each other and to the MT channel flow profile for $y^+ > 10$, while in the near-wall region the IWHF turbulent transport is sensibly smaller, due to the lower correlation between radial velocity and temperature. The gradient transport model has been widely used to calculate the turbulent transport term:

$$\overline{u_r^{+\prime}\vartheta^{+\prime}\vartheta^{+\prime}} \approx \frac{2}{Re^*}\frac{\alpha_t}{\nu}\frac{\mathrm{d}k_\vartheta^+}{\mathrm{d}\hat{r}}$$

From the present DNS data, Figure 8(e), it is evident that the model leads to a quite accurate representation of $\overline{u_r^{+\prime}\vartheta^{+\prime}\vartheta^{+\prime}}$ and the extrema of k_ϑ^+, located at $y^+ \approx 16.1, 21.1, 19.3$ for the IWHF, IWT and MT cases, are in good agreement with the zeroes of $\overline{u_r^{+\prime}\vartheta^{+\prime}\vartheta^{+\prime}}$, located at $y^+ \approx 16.0, 19.7, 18.5$, respectively. This rough agreement has been evidenced also by Na *et al.* [20] in their simulation of a turbulent channel flow with two walls at constant, different temperatures.

The molecular diffusion term has the same qualitative behaviour as the turbulent transport term, in that it carries turbulent thermal fluctuations towards the wall and the core region, from the region of maximum P_{k_ϑ}. However, D_{k_ϑ} does not vanish at the wall, where it balances dissipation. In the near-wall region, the molecular diffusion term for the IWHF case is sensibly less intense than for the other boundary conditions, due to the lack of the temperature front.

The dissipation term is strongly affected by the boundary conditions. The IWT case shows the most intense dissipation. In the near-wall region the IWHF dissipation decreases significantly, since its major contribution, the term containing the radial derivative, is damped according to the imposed isoflux condition. The dissipation for the pipe flow with MT wall thermal conditions is slightly more intense than for the channel flow. It is usual practice to define a modified dissipation $\tilde{\varepsilon}_\vartheta$, which does not include the effect of the oscillations in time of the instantaneous temperature profile in the near-wall region:

$$\tilde{\varepsilon}_\vartheta^+ = \varepsilon_\vartheta^+ + \frac{1}{Pr}\left[\frac{\partial\sqrt{\overline{(\vartheta^{+\prime})^2}}}{\partial y^+}\right]^2$$

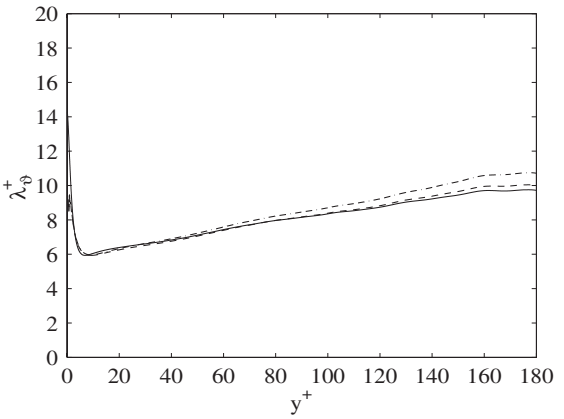

Figure 9. Taylor microscale λ_ϑ^+. ——: IWHF; – – –: MT; — · ——: IWT.

A Taylor microscale λ_ϑ^+ for the dissipation of k_ϑ^+ can be defined as

$$\tilde{\varepsilon}_\vartheta^+ = \frac{1}{Pr}\frac{\overline{(\vartheta^{+\prime})^2}}{2}\left(\frac{1}{\lambda_\vartheta^+}\right)^2$$

Values of λ_ϑ^+ are presented in Figure 9, where a weak dependence on the wall thermal boundary conditions can be observed for $y^+ > 20$, while in the conduction sublayer the IWHF Taylor microscale is much larger, since turbulent thermal fluctuations generated in the buffer region can reach the wall without relevant damping.

3.7. Two-point correlations and spectra

Figure 10(a) shows the autocorrelation function with streamwise separation for the fluctuating velocity components at $y^+ \approx 40$. The corresponding data by Fukagata *et al.* [15] are reported for comparison. Despite a generally good agreement for $\Delta x^+ \leqslant 400$, the present autocorrelations for u_x' fall off more rapidly at larger separations and essentially vanish within half domain length, suggesting that the adopted pipe length is (marginally) sufficient to capture the largest scale structures of the flow field. Figure 10(b) shows the autocorrelation function with streamwise separation for the temperature fluctuations at $y^+ \approx 10, 40$. Non-zero correlations are obtained at half pipe length at both $y^+ \approx 40$ and $y^+ \approx 10$, particularly with the IWHF condition, showing that the computational domain is only marginally adequate for the simulation of the temperature field. The minimum in the azimuthal autocorrelation function for the temperature fluctuations at $y^+ \approx 11$ reveals that the spacing between the thermal streaks equals 106 wall units for the MT and IWT cases, while a slightly larger separation of 118 is obtained for the IWHF case.

Figures 11(a) and 11(b) present the streamwise energy spectra, scaled by the corresponding r.m.s. values, at $y^+ \approx 5$ and $y^+ \approx 23$. At $y^+ \approx 5$ the spectrum for the IWHF temperature fluctuations decays faster than the others. This feature is consistent with the larger values of λ_ϑ^+ at the wall, for the IWHF case. For $y^+ \approx 23$ the energy spectra for the three cases are coincident, showing that, in the outer region, the intensity of the three temperature fluctuations is different but similarly distributed among wavenumbers. This is particularly evident for the

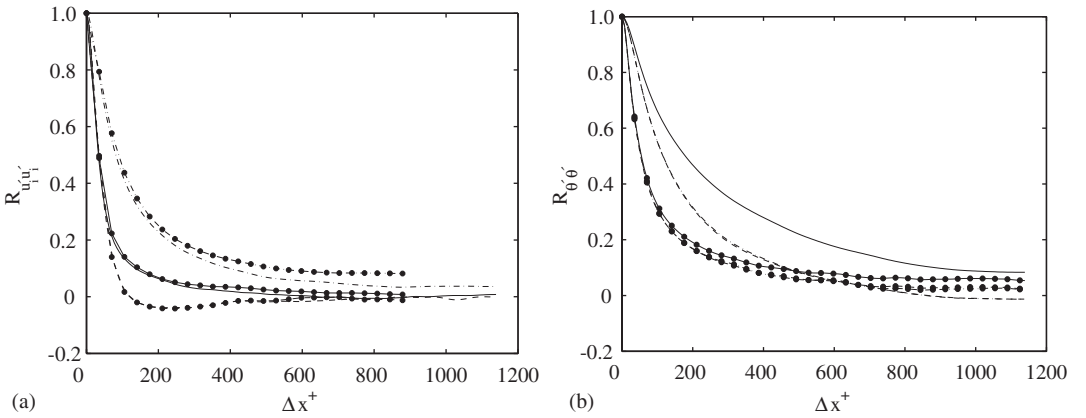

Figure 10. Autocorrelation functions with streamwise separation for: (a) the fluctuating velocity components; and (b) the temperature fluctuations. Conventions used in (a); lines: present DNS at $y^+ \approx 40$; lines with symbols: Fukagata *et al.* [15] at $y^+ \approx 40$; ——: $R_{u_r' u_r'}$; – – –: $R_{u_\varphi' u_\varphi'}$; — · —: $R_{u_x' u_x'}$. Conventions used in (b); lines: present DNS at $y^+ \approx 10$; lines with symbols: present DNS at $y^+ \approx 40$; ——: IWHF; – – –: MT; — · —: IWT.

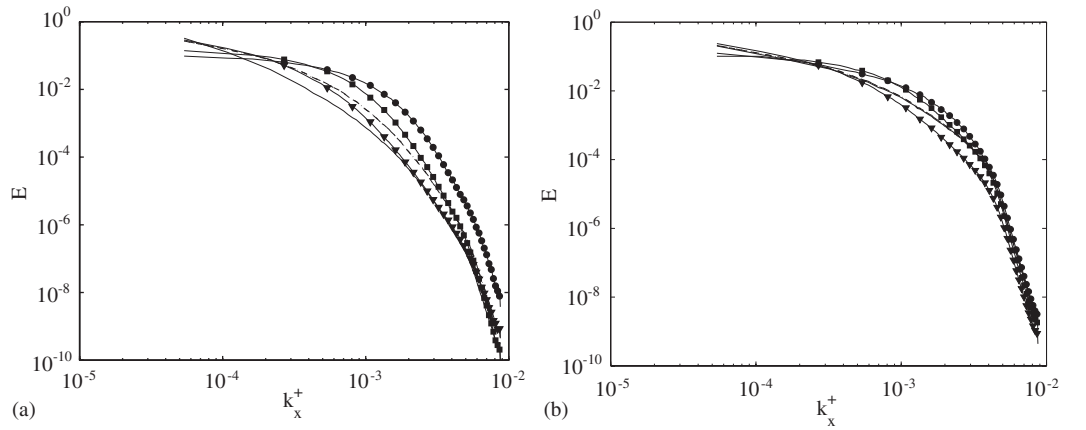

Figure 11. Streamwise energy spectra at: (a) $y^+ \approx 5$; and (b) $y^+ \approx 23$. ——: E_ϑ for IWHF; – – –: E_ϑ for MT; — · —: E_ϑ for IWT; —●—: E_{u_r}; —■—: E_{u_φ}; —▼—: E_{u_x}.

MT and IWT cases, whose energy spectra are almost coincident at all distances from the wall. The spanwise spectra, not reported here, reveal a similar behaviour. The normalized spectrum of u_x' is almost coincident with the spectra of ϑ' for the MT and IWT cases in a range of low wavenumbers, containing about 85% of the total $\overline{\vartheta'^2}$; at larger wavenumbers, the streamwise velocity spectrum decays faster than the temperature spectrum for the MT and IWT cases. As for the IWHF spectrum, in a wide range of low wavenumbers, containing most of the total $\overline{\vartheta'^2}$, the spectral temperature modes are weaker than the corresponding streamwise velocity modes; at the largest wavenumbers the spectra of u_x' and the IWHF ϑ' tend to collapse.

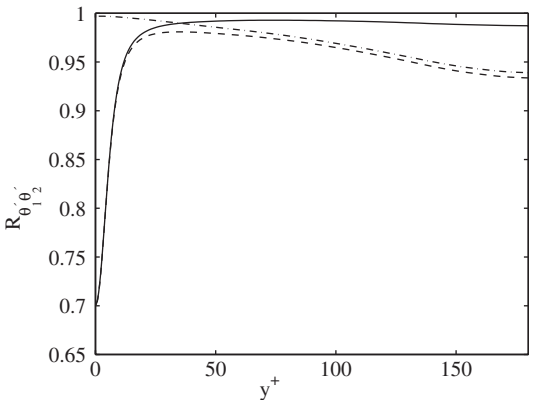

Figure 12. One-point mutual correlation coefficients for the three considered temperature fields. – – –: $R_{\mathrm{IWHF-IWT}}$; ——: $R_{\mathrm{IWHF-MT}}$; — · —: $R_{\mathrm{IWT-MT}}$.

3.8. *Correlation coefficients between different temperature fields*

The similarity between the three considered temperature fields can be quantified by the one-point mutual correlation coefficients, shown in Figure 12. The IWT–MT correlation coefficient is close to unity in the inner layer, while a rapid decay can be observed for the IWHF–MT and IWHF–IWT correlation coefficients approaching the wall. It confirms that, in this region, the dominant distinctive characteristic of the thermal boundary conditions consists in allowing or avoiding the wall temperature fluctuations. The correlation coefficients behave differently in the outer layer, where the correlation between the IWHF and the MT temperature fluctuations increases towards the centreline, while the correlation of the IWT with the other temperature fluctuations decreases. These observations support the thesis that, in the outer layer, the differences between the three turbulent thermal fields are mainly dictated by the different axial variation of the mean temperature or, ultimately, by the different distribution of the heat flux, released from the wall. Although in the outer layer all the correlation coefficients are no smaller than 0.95, the observation that the IWT–IWHF correlation decays towards the centreline confirms that the differences between isothermal and isoflux wall thermal conditions are not confined to the inner layer. The physical intuition that the MT conditions are somehow intermediate between ideal isothermal and ideal isoflux conditions is confirmed by the present results: while the MT and IWT temperature fluctuations are highly correlated in the inner layer, a very large correlation is attained between the IWHF and MT fluctuations in the outer layer.

4. CONCLUDING REMARKS

Direct numerical simulations for turbulent flow and heat transfer are performed for three different wall thermal conditions and their effect on the turbulence quantities is investigated. Results from previous studies [3, 4] suggest that the influence of MT or IWHF boundary conditions is confined to the conduction sublayer and that even more general wall thermal conditions have only a weak effect on the distribution of relevant heat transfer parameters like

the turbulent Prandtl number [20]. An original outcome of this research is the observation that the damping of the temperature fluctuations at the wall is effective in the inner layer, while the axial distribution of the wall heat flux is more influent in the core region. According to findings by Kong *et al.* [4] and Tiselj *et al.* [3], the present results show that the imposition of either MT or IWHF conditions affects the temperature statistics only within the conduction sublayer, while the IWT conditions, not considered in References [3, 4], cause differences with respect to the other conditions up to the core region. In order to synthetically quantify the similarity between the three considered temperature fields, a mutual correlation coefficient is introduced; its distribution suggests that the MT condition, commonly used in DNS studies of fully developed turbulent heat transfer with isothermal walls, acts as ideal isothermal conditions in the inner layer and as ideal isoflux conditions in the outer layer. The spectral distribution of the temperature fluctuations reveals that, out of the inner layer, the temperature fluctuations for the three considered boundary conditions are almost identically distributed among wavenumbers, while in the inner layer the ideal isoflux temperature fluctuations decay faster at the largest wavenumbers. To investigate the differences between fully developed turbulent heat transfer in axisymmetric pipe and plane channel geometry, the present DNS results are compared to those obtained from channel flow simulations. The differences between channel and pipe flow statistics with MT boundary conditions are modest and reveal that the temperature fluctuations in the pipe are slightly more intense.

ACKNOWLEDGEMENTS

Financial support for this research was provided by MIUR-PRIN 2001, Convezione Monofase Naturale e Mista: Aspetti Fondamentali ed Applicazioni in Componenti e Sistemi Termici, and is gratefully acknowledged. The author particularly thanks Dr E. Stalio and Dr G. Moncalvo for valuable comments and good discussions.

REFERENCES

1. Kim J, Moin P. Transport of passive scalars in a turbulent channel flow. *Turbulent Shear Flows* 1989; **VI**:85–96.
2. Kasagi N, Tomita Y, Kuroda A. Direct numerical simulation of passive scalar field in a turbulent channel flow. *Journal of Heat Transfer* (ASME) 1992; **114**:598–606.
3. Tiselj I, Pogrebnyak E, Li C, Mosyak A, Hetsroni G. Effect of wall boundary condition on scalar transfer in a fully developed turbulent flume. *Physics of Fluids* 2001; **13**(4):1028–1039.
4. Kong H, Choi H, Lee JS. Direct numerical simulation of turbulent thermal boundary layers. *Physics of Fluids* 2000; **12**(10):2555–2568.
5. Piller M, Nobile E, Hanratty TJ. Direct numerical simulation of turbulent transport at low Prandtl numbers in a channel flow. *Journal of Fluid Mechanics* 2002; **458**:419–441.
6. Seki Y, Abe H, Kawamura H. DNS of turbulent heat transfer in a channel flow with different thermal boundary conditions. *Proceedings of the 6th ASME-JSME Thermal Engineering Joint Conference*, Hawaii, U.S.A., 2003.
7. Jakob M. *Heat Transfer*. Wiley: New York, 1958.
8. Sommer TP, So RMC, Zhang HS. Heat transfer modeling and the assumption of zero wall temperature fluctuations. *Transactions of ASME*, *sez. C*: *Journal of Heat Transfer* 1994; **116**:855–863.
9. Patankar SV, Liu CH, Sparrow EM. Fully developed flow and heat transfer in ducts having streamwise-periodic variations of cross-sectional area. *Journal of Heat Transfer* 1977; **99**:180–186.
10. Griffin MD, Jones E, Anderson JD. A computational fluid dynamics technique valid at the centreline for non-axisymmetric problems in cylindrical coordinates. *Journal of Computational Physics* 1979; **30**:352–360.
11. Akselvoll K, Moin P. An efficient method for temporal integration of the Navier–Stokes equations in confined axisymmetric geometries. *Journal of Computational Physics* 1996; **125**:454–463.
12. Ferziger J, Perić M. *Computational Methods for Fluid Dynamics*. Springer: New York, 1999.

13. Gresho PM. On the theory of semi-implicit projection methods for viscous incompressible flow and its implementation via a finite element method that also introduces a nearly consistent mass matrix. Part I: theory. *International Journal for Numerical Methods in Fluids* 1990; **11**:587–620.
14. Grötzbach G. Spatial resolution requirements for direct numerical simulation of the Rayleigh–Benard convection. *Journal of Computational Physics* 1983; **49**:241–264.
15. Fukagata K, Kasagi N. Highly energy-conservative finite difference method for the cylindrical coordinate system. *Journal of Computational Physics* 2002; **181**:478–498.
16. Eggels J, Unger F, Weiss M, Westerweel J, Adrian R, Friedrich R, Nieuwstadt F. Fully developed turbulent pipe flow: a comparison between direct numerical simulation and experiment. *Journal of Fluid Mechanics* 1994; **268**:175–209.
17. Kakac S, Shah R, Aung W. *Handbook of Single-Phase Convective Heat Transfer*. Wiley: New York, 1987.
18. Subramanian CS, Antonia RA. Effect of Reynolds number on slightly heated turbulent boundary layer. *International Journal of Heat and Mass Transfer* 1981; **24**(11):1833–1846.
19. Johnk RE, Hanratty TJ. Temperature profiles for turbulent flow of air in a pipe. I—the fully developed heat transfer region. *Chemical Engineering Science* 1962; **17**:867–881.
20. Na Y, Papavassiliou DV, Hanratty TJ. Use of direct numerical simulation to study the effect of Prandtl number on temperature fields. *International Journal of Heat and Fluid Flow* 1999; **20**:187–195.
21. Kawamura H, Abe H, Matsuo Y. DNS of turbulent heat transfer in channel flow with respect to Reynolds and Prandtl number effects. *International Journal of Heat and Fluid Flow* 1999; **20**:196–207.
22. Abe H, Kawamura H, Kuroda H. Direct numerical simulation data base for turbulent channel flow with heat transfer. Turbulent poiseuille flow. $Re_\tau = 180$, $Pr = 0.71$, fourth-order finite-difference scheme with $256 \times 128 \times 256$, 2003.
23. Abe H, Kawamura H. A study of turbulence thermal structure in a channel flow through dns up to $Re_\tau = 640$ with $Pr = 0.025$ and 0.71. In *Proceedings of 9th European Turbulence Conference*, Castro I, Hancock P, Thomas T (eds), 2002; 399–402.
24. Chen CHP, Blackwelder RF. Large scale motion in a turbulent boundary layer: a study using temperature contamination. *Journal of Fluid Mechanics* 1978; **89**(1):1–31.
25. Elena M. Etude experimentale de la turbulence au voisinage de la paroi d'un tube legerement chauffe. *International Journal of Heat and Mass Transfer* 1977; **20**:935–944.
26. Blackwelder RF, Kaplan RE. Intermittent structures in turbulent boundary layers. *Proceedings of Meeting Agard*, London, 1971.

